Earthquakes and Structures, *Vol. 15, No. 3 (2018) 263-273*
DOI: https://doi.org/10.12989/eas.2018.15.3.263

Enhanced least square complex frequency method for operational modal analysis of noisy data

V. Akrami[*1] and S. Majid Zamani[2a]

[1]*Faculty of Engineering, University of Mohaghegh Ardabili, Ardabil, Iran*
[2]*Structural Engineering Department, Road, Housing and Urban Research Center, Tehran, Iran*

(Received September 24, 2017, Revised June 2, 2018, Accepted June 10, 2018)

Abstract. Operational modal analysis is being widely used in aerospace, mechanical and civil engineering. Common research fields include optimal design and rehabilitation under dynamic loads, structural health monitoring, modification and control of dynamic response and analytical model updating. In many practical cases, influence of noise contamination in the recorded data makes it difficult to identify the modal parameters accurately. In this paper, an improved frequency domain method called Enhanced Least Square Complex Frequency (eLSCF) is developed to extract modal parameters from noisy recorded data. The proposed method makes the use of pre-defined approximate mode shape vectors to refine the cross-power spectral density matrix and extract fundamental frequency for the mode of interest. The efficiency of the proposed method is illustrated using an example five story shear frame loaded by random excitation and different noise signals.

Keywords: Operational Modal Analysis (OMA); ambient vibration; frequency domain; Least Square Complex Frequency (LSCF) method; mode shape; noise signal

1. Introduction

Since early 1990's, operational modal analysis (OMA) has drawn great attention in civil engineering community with applications for off-shore platforms, buildings, towers, bridges, etc (Zhang *et al*. 2005). OMA techniques are used to identify the modal characteristics of the system where only the structural output (response of the structure in operational condition subjected to ambient vibrations) is known. These estimates of the modal parameters can be used directly or within a model updating framework (Papadimitriou and Papadioti 2013, Zhang and Au 2016, Zhang *et al*. 2017, Jensen *et al*. 2017) for the assessment and control of vibrations, the rehabilitation or optimization of design, and the monitoring of performance and health state of structures (Ni *et al*. 2015, Zhang *et al*. 2016, Aras 2016). An inclusive summary of OMA techniques is provided by Rainieri and Fabbrocino (2014).

During the past few years there have been many studies conducted on different methods and applications of OMA and hundreds of articles have been published in this field (Masjedian and Keshmiri 2009). Peeters and De Roeck (2001) have reviewed some of these modeling techniques, including: state-space models, Auto-Regressive Moving Average (ARMA) models, and frequency-domain models. With the development of operational modal analysis, the advantages of using system identification methods that can deal well with the high 'noise' levels that are met in operational conditions, became clear (Reynders 2012). In this regard, ARMA methods aimed at modeling the dynamics of both the structural system and the noise (Rainieri and Fabbrocino 2014). These methods assume that the system input as well as the measurement noises has a continuous white noise nature. However, as these noises are not perfectly white (Reynders 2012), nonwhite system input and output measurement noises become part of the identified system resulting in lots of additional spurious poles, not related to the dynamics of the system under study.

Different authors have developed theoretical models or stepwise algorithms to overcome this problem. Among the rest, Mohanty and Rixen (2004) have studied OMA in the presence of harmonic excitation. For this purpose, they have introduced a modification to the least-square complex exponential (LSCE) identification procedure to include explicitly the harmonic component. Rodrigues *et al*. (2004) have explored the idea of applying the random decrement (RD) functions for spectral estimation to be used in frequency domain OMA methods. Since the experimentally measured structural responses always have some noise content, the time segments averaging of the RD technique, reduces the noise in the resulting RD functions. Peeters *et al*. (2007) have introduced a harmonic filtering method to filter disturbing harmonics from broadband time data. The proposed technique works at four steps: a) estimating the fundamental harmonics of the system; b) re-sampling the data in angle domain; c) applying synchronous averaging to remove the harmonics; and d) restoring the signal in time domain. Shouyuan *et al*. (2008) developed a method for distinguishing harmonic noise modes from measured vibration signal based on the differences of the statistical properties of a stochastic signal and a harmonic signal.

∗Corresponding author, Assistant Professor
E-mail: v.akrami@uma.ac.ir
[a]Assistant Professor

http://www.techno-press.com/journals/eas&subpage=7
ISSN: 2092-7614 (Print), 2092-7622 (Online)

Also, they have used the channel projection technique to reduce noise modes caused by random errors. Gouache *et al*. (2013) have used phase analysis adapted to a transient context to conduct operational modal analysis under a harmonic transient input. Bonness and Jenkins (2015) have presented a noise removal technique based on coherent output power (COP) between the recorded signal and the reference noise signal. The proposed technique has been demonstrated using vibration data and dynamic wall pressure measurements from a thin-walled aluminium cylinder filled with flowing water. Following the research conducted by Yu and Ren (2005), Qin *et al*. (2015) investigated output-only modal analysis for bridge structures by using an improved version of empirical mode decomposition (EMD). This is done by means of a bandwidth restricted EMD for decomposing non-stationary output measurements. The modal parameters are extracted by both random decrement technique and stochastic subspace identification. Recently, Ong *et al*. (2017) used impact-synchronous modal analysis (ISMA) for filtering out the non-synchronous cyclic load component, its harmonics, and noises. The Bayesian approach for operational modal analysis is another method for modal identification that accounts for the effect of measurement noise analytically (Au 2017). Zhang *et al*. (2018) and Ni *et al*. (2017) used this method for operational modal analysis of high-rise buildings.

As mentioned, for an effective identification of modal parameters, it is necessary to ensure that the recorded data has a good signal-to-noise ratio (Brincker *et al*. 2003). However, in many practical cases, influence of noise contamination in the recorded data makes it difficult to identify the modal parameters accurately. As in most cases, a good estimation of structural mode shapes is available prior to ambient vibration tests, this information may be used to handle noisy data and extract corresponding modal parameters during OMA. This paper presents an enhanced version of LSCF method for determination of vibration properties from noisy data based on the selected mode shape vector. For this purpose, a vector containing the correlation between predicted and measured cross-power spectral density (C-PSD) matrices is used to refine the measured data and eliminate effect of unwanted noises. The efficiency of the proposed method is illustrated using an example five story shear frame loaded by random excitation and different noise signals.

2. Theory

2.1 Least square complex frequency method

The Least Squares Complex Frequency (LSCF) method, starts from a scalar matrix-fraction description (better known as a common-denominator model) for the measured set of cross-power spectral densities (C-PSD). This method is basically a curve-fitting technique based on the minimization of an equation error between the measured and the predicted PSD matrix. For a generic couple k of output channels (k=1, 2, …, $l\times l$), the cross-power spectrum at frequency line f (f=1, 2, …, N_f) can be estimated using a common-denominator model (Rainieri and Fabbrocino 2014)

$$G_k(\omega_f) = \frac{\sum_{j=0}^{n} \theta_{k,j}\Omega_f^j}{\sum_{j=0}^{n} \psi_j \Omega_f^j} \tag{1}$$

where, the coefficients $\theta_{k,j}$ and ψ_j are the unknown parameters to be estimated; n is the order of numerator and denominator polynomials; Ω_f is the generalized transform variable which for discrete-time domain is evaluated as: $\Omega_f = e^{i\omega_f \Delta t}$; and Δt is the sampling interval. The coefficients $\theta_{k,j}$ and ψ_j are obtained as a solution of a linear least squares problem defined by the following equations

$$\varepsilon_k(\omega_f) = \sum_{j=1}^{n} \theta_{k,j}\Omega_f^j - \hat{G}_k(\omega_f) \times \sum_{j=1}^{n} \psi_j \Omega_f^j \tag{2}$$

where, $\hat{G}_k(\omega_f)$ is the cross-power spectrum at frequency line for the k-th couple of output channels. As above equations are linear in the parameters, they can be re-formulated in the matrix form

$$\{\varepsilon_{k,i}\} = [J]\begin{Bmatrix}\theta_{k,j}\\ \psi_{k,j}\end{Bmatrix}$$

$$\begin{Bmatrix}\{\varepsilon_{1,1\ldots N_f}\}\\ \{\varepsilon_{2,1\ldots N_f}\}\\ \vdots \\ \{\varepsilon_{l.l,1\ldots N_f}\}\end{Bmatrix} = \begin{bmatrix}[\Gamma_1] & [0] & \cdots & [0] & [\Upsilon_1]\\ [0] & [\Gamma_2] & \ddots & [0] & [\Upsilon_2]\\ \vdots & \vdots & \ddots & \vdots & \vdots\\ [0] & [0] & \cdots & [\Gamma_{l.l}] & [\Upsilon_{l.l}]\end{bmatrix}\begin{Bmatrix}\{\theta_{1,1\ldots n}\}\\ \{\theta_{2,1\ldots n}\}\\ \vdots\\ \{\theta_{l.l,1\ldots n}\}\\ \{\psi_{1\ldots n}\}\end{Bmatrix} \tag{3}$$

where, i=1,…,N_f; j=0,…,n and Γ_k and Y_k are $N_f\times(n+1)$ matrices defined as it follows

$$\Gamma_k(i,j) = e^{(i\omega_i \Delta t)j} \tag{4}$$

$$\Upsilon_k(i,j) = -\hat{G}_k(\omega_i)\cdot e^{(i\omega_i \Delta t)j} \tag{5}$$

The unknown parameters can be estimated directly from the Jacobian matrix [J] of Eq. (3). However, most estimators used in operational modal analysis form the normal equations explicitly, i.e., they compute $[J]^H[J]$ as this results in a significant reduction in computational time and faster implementation (where, ^{H} is the sign of Hermitian adjoint). The reduced normal equations are given as

$$[M]\{\psi_{1\ldots n}\} = \left[\sum_{k=1}^{l\times l}[T_k] - [S_k]^H[R_k]^{-1}[S_k]\right]\{\psi_{1\ldots n}\} \approx 0 \tag{6}$$

where

$$[R_k] = [\Gamma_k]^H[\Gamma_k] \tag{7}$$

$$[S_k] = [\Gamma_k]^H[\Upsilon_k] \tag{8}$$

$$[T_k] = [\Upsilon_k]^H[\Upsilon_k] \tag{9}$$

When [M] is calculated, it can be used to find $\{\psi_{1..n}\}$ as

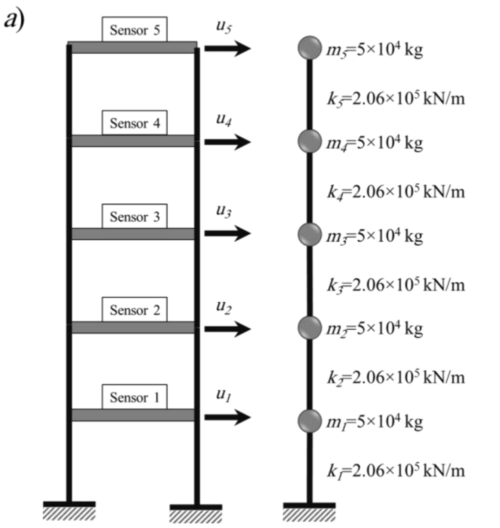

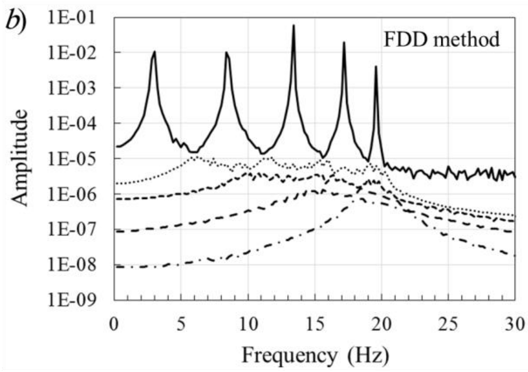

Mode	Natural frequency (Hz)
1	2.91
2	8.49
3	13.38
4	17.19
5	19.60

Fig. 1 Dynamic properties of the reference model; (a) mass and stiffness of stories; (b) natural frequencies (FDD method)

given by the following equation

$$\{\psi_{1\ldots n}\} = \begin{Bmatrix} -\left[M(1:n,1:n)\right]^{-1}.\left[M(1:n,n+1)\right] \\ 1 \end{Bmatrix} \tag{10}$$

Once the coefficients $\{\psi_{1..n}\}$ have been computed, the poles in the z-domain can be obtained as the roots of the denominator polynomial (z_r). Then the natural frequency and the damping ratio of the r-th mode can be computed as follows

$$f_r = \frac{|\ln(z_r)|}{2\pi.\Delta t} \tag{11}$$

$$\xi_r = -\frac{\mathrm{Re}[\ln(z_r)]}{|\ln(z_r)|} \tag{12}$$

As the natural frequency and damping ratio become known, mode shapes can be obtained as a solution of a second least squares problem. For more information on determination of mode shapes one can refer to Rainieri and Fabbrocino (2014).

2.2 Enhanced LSCF method

As mentioned before, the proposed method makes the use of pre-defined approximate mode shape vectors to refine the cross-power spectral density matrix. For this purpose, suppose that $1\times l$ vector, ϕ, is the mode shape vector corresponding to the r-th vibration mode. The outer product of this vector with itself, $\{\phi\}\{\phi\}^{\mathrm{T}}$, will be an $l\times l$ matrix holding the information about auto- and cross-spectral densities of output channels at r-th vibration mode. The correlation between this matrix and the measured PSD matrix will be maximised near the r-th fundamental frequency since at this frequency the residue matrix will generally hold the information about the r-th mode shape vector. Meanwhile at other frequencies corresponding to noise, harmonic or other structural modes the correlation between these matrices will tend to zero. Hence this quantity can be treated as an index, namely the Correlation Index (CI), to refine the PSD matrix used by LSCF method. In order to calculate CI for a given mode shape vector, the elements of $\{\phi\}\{\phi\}^{\mathrm{T}}$ matrix should be stored in an $(l\times l)\times 1$ vector as per the following equation

$$\Phi_k = \phi_m.\phi_n \quad , \quad \begin{cases} m = \mathrm{int}(k/l)+1 \\ n = k - \mathrm{int}(k/l)\cdot l \end{cases} \tag{13}$$

where, int(-), stands for the integer function. The correlation between this vector and the PSD matrix at each frequency can be estimated using

$$CI(\omega_f) = \left\{ \frac{\left|\{\Phi_k\}^H \{\hat{G}_k(\omega_f)\}\right|^2}{(\{\Phi_k\}^H\{\Phi_k\})\cdot(\{\hat{G}_k(\omega_f)\}^H\{\hat{G}_k(\omega_f)\})} \right\}^{\alpha} \tag{14}$$

where the exponent, α, is used to calibrate the sensitivity of the method. As the $CI(\omega_f)$ vector of dimension $N_f\times 1$ is calculated, the Eq. (5) can be re-written as

$$\mathrm{Y}_k(i,j) = -CI(\omega_i)\cdot \hat{G}_k(\omega_i)\cdot e^{(\mathrm{i}\omega_i\Delta t)j} \tag{15}$$

Application of this modified equation inside the framework of LSCF will result in an enhanced method which is capable of detecting the fundamental frequency corresponding to the adopted mode shape vector, by neglecting the peaks corresponding to noise and harmonic modes or even other structural poles.

The sensitivity exponent, α, in Eq. (14) can take different values, changing the applicability of the proposed method. Using, α=0, the enhanced method will be simplified to traditional LSCF method. For an, α, value greater than zero, the correlation index will refine the PSD matrix. As the sensitivity exponent, α, increases the effect of selected mode shape vector will become more obvious. It is worthy to mention that if the parameter α is set to unity, the calculated *CI* will be somehow analogues to Modal Assurance Criteria (MAC) used in traditional OMA. A negative value for α may be used to remove the noise or harmonic modes with a known mode shape vector.

The proposed method can be made even more efficient by introducing a *CI* rejection level defined as

$$CI_{new}(\omega_f) = \begin{cases} 0 & CI_{old}(\omega_f) < 0.5 \\ 1 & CI_{old}(\omega_f) \geq 0.5 \end{cases} \tag{16}$$

However, as LSCF method is basically a curve-fitting technique, adoption of *CI*=0 for a wide range of frequencies may result in a numerical error. To avoid this problem, Eq. (15) may be modified as

$$\mathrm{Y}_k(i,j) = -\max\{CI(\omega_i)\cdot \hat{G}_k(\omega_i),\ \varepsilon\}\cdot e^{(\mathrm{i}\omega_i\Delta t)j} \tag{17}$$

where, ε, is a positive small value compared to other values in PSD matrix. In this study the value of, ε, is assumed to be equal to: $10^{-6}\max\{\hat{G}_k(\omega_f)\}$. Effect of this parameter is discussed in sec. 3.3.1.

3. Discussion on the application of eLSCF

3.1 Description of reference structure

A five story shear frame is selected as the reference model to evaluate performance of eLSCF method. The mass and stiffness of all stories are assumed to be identical as shown in Fig. 1(a). The arrangement of sensors is shown in the figure. The model is loaded using a white noise composed of 100,000 data points (100 sec) and the acceleration responses at different story levels is used as the input to LSCF and eLSCF methods. Fig. 1(b) displays application of well-known Frequency Domain Decomposition (FDD) method to the response of the reference model. Natural frequencies corresponding to each mode is summarized in Fig. 1(c).

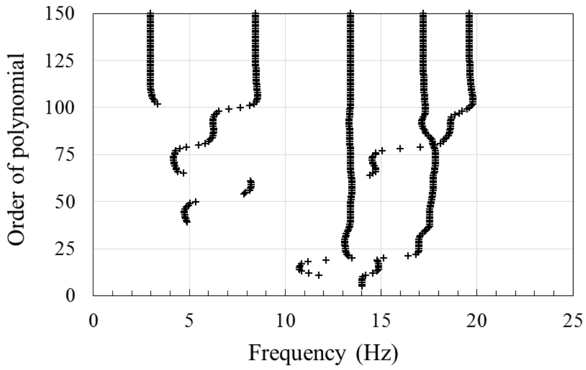

Fig. 2 Stabilization of natural frequencies for the reference model obtained from LSCF method

3.2 Application of exact mode shapes

In the first phase, the capability eLSCF in detection of modal frequencies is evaluated and compared to the results obtained from traditional LSCF. Fig. 2 displays stabilization diagram from LSCF method used for detecting natural frequencies of the reference model. As it can be seen in the figure, when the order of system is below 100, only two modes (third and fourth) are detectable and other modes are missing. However as the order of system increases above this value, all modal frequencies start to stabilize. In fact, as

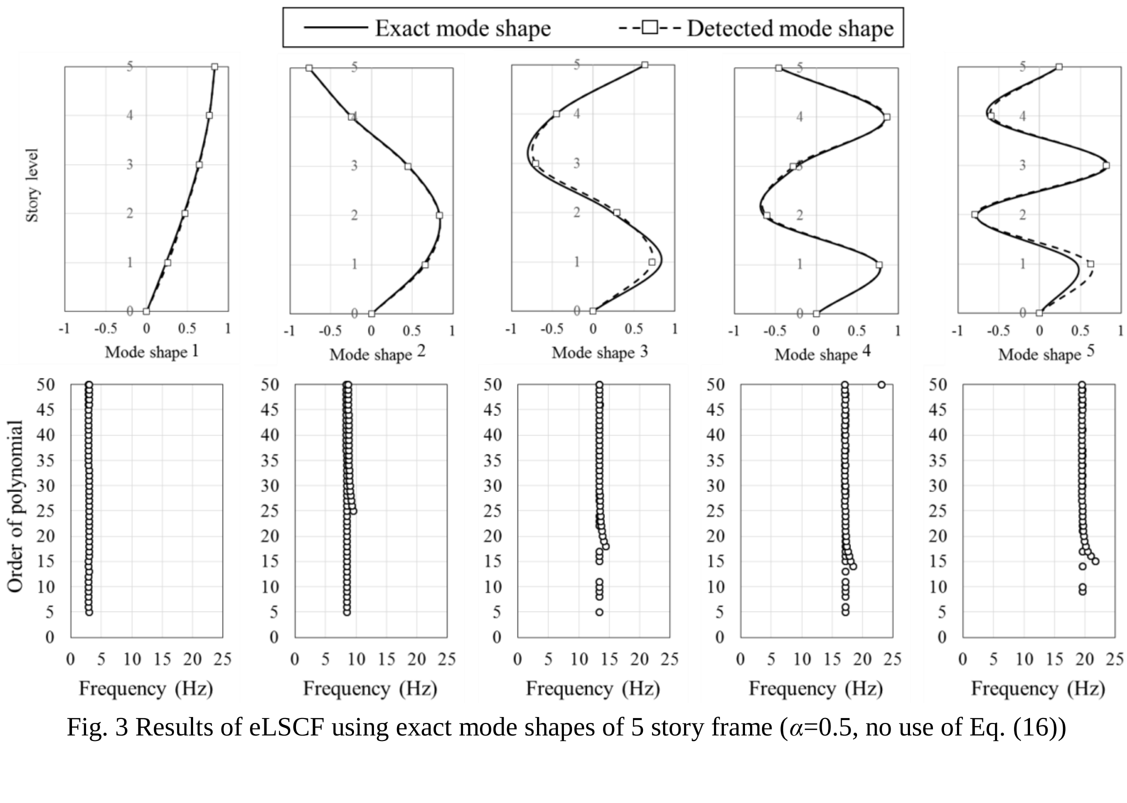

Fig. 3 Results of eLSCF using exact mode shapes of 5 story frame (α=0.5, no use of Eq. (16))

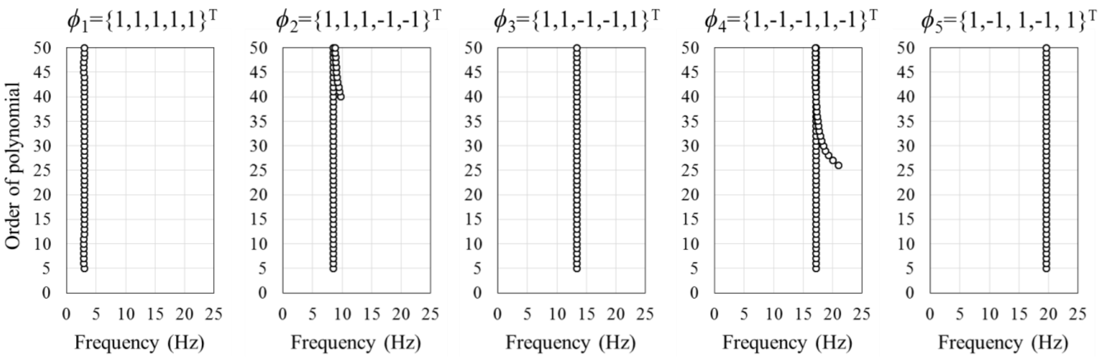

Fig. 4 Results of eLSCF using the approximate mode shapes for 5 story frame (α=1.0, using Eq. (16))

the selected structure has more degrees of freedom, the stabilization of all modes will require even a larger system order (Schanke 2015).

As described before, an estimate of mode shape vectors for the target fundamental modes is needed prior to the extraction of modal frequencies using eLSCF. For the first attempt, the exact mode shapes of the reference model are calculated from modal analysis and used as an input to eLSCF. Fig. 3 displays adopted mode shapes and stabilization diagrams for the corresponding fundamental frequencies. To extract the plots of Fig. 3, the value of α is assumed to be 0.5, and no use made of Eq. (16). According to the figure, the proposed eLSCF method is very successful in detection of target modal frequencies. It is worthy to note that the stabilization of diagrams starts even with a very low system order which shows the computational efficiency of the method.

3.3 Application of approximate mode shapes

As in the case of real structures (building, bridge, dam, etc.) the exact mode shape corresponding to the target fundamental frequency is not usually available, it is important to evaluate efficiency of the proposed method where the approximate mode shape vectors are being used.

3.3.1 Detection of modal frequencies

Fig. 4 displays results of eLSCF using the approximate mode shapes for the reference model. Graphs are obtained using Eq. (16) and assuming α=1.0. As it can be seen in the figure, the enhanced method is capable of detecting modal frequencies even if the input mode shape vector is approximate. However, it should be noted that when the similarity between the assumed and actual modal vectors is very low, the correlation index around the target frequency (calculated from Eq. (14)) may be less than the *CI* rejection level used in Eq. (16), resulting in a numerical error.

As an example, assuming that the modal vector corresponding to the first fundamental frequency is equal to ϕ_1={1, 0.92, 0.76, 0.55, 0.28}^{T} (i.e., inverse of the first mode shape) the value of *CI* will be less than 0.5 around the first structural pole. Usually, adoption of a lower value for parameter α or a lower *CI* rejection level can solve this problem (in the case of above example the first pole will stabilize using α=0.45). However, this can cause detection of additional unwanted poles, too.

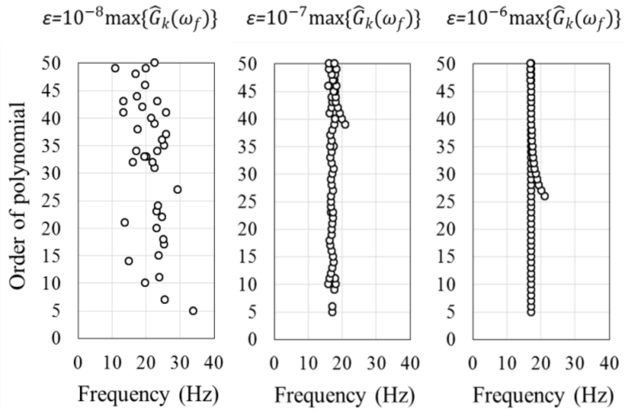

Fig. 5 Effect of parameter, ε, on stabilization of the fourth mode

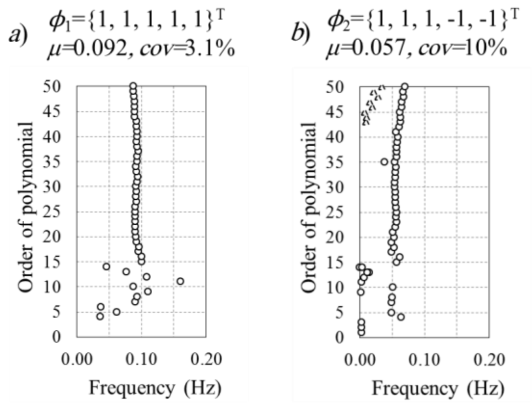

Fig. 6 Stabilization of damping ratio for the second model in Table 1

Another parameter that can affect efficiency of the proposed method is the parameter, ε, introduced in Eq. (17). This parameter will be used when the *CI* rejection level defined by Eq. (16) is being utilized. Fig. 5 shows effect of this parameter on stabilization of the fourth mode. Graphs are obtained using α=1.0 and approximate mode shape vector ϕ_4={1, -1, -1, 1, -1}^{T}. According to the figure, when the parameter, ε, is very close to zero the target frequency may not stabilize due to the numerical problems. However, as this parameter increases, the proposed method gives more clear stabilization diagrams. For the model studied in this paper, the smallest suitable value of this parameter is

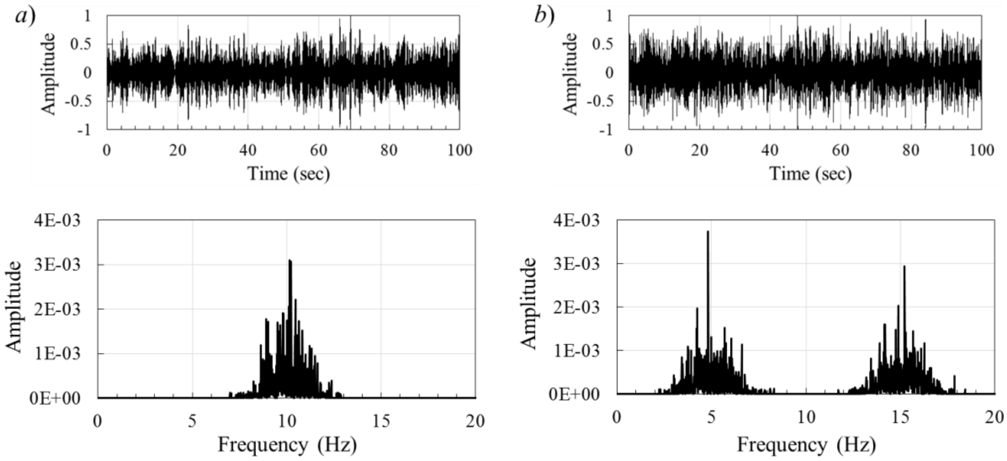

Fig. 7 Sample noise signals; (a) noise with μ_f=10 Hz and σ_f=1 Hz; (b) noise with μ_{f1}=5 Hz, μ_{f2}=10 Hz, $\sigma_{f1,2}$=1 Hz

Table 1 Comparison of exact and predicted damping ratios

	First Mode			Second Mode		
	Exact	Predicted		Exact	Predicted	
		mean	cov		mean	cov
Model 1	0.05	0.043	5%	0.02	0.018	21%
Model 2	0.1	0.092	3.1%	0.06	0.057	10%

found to be: $10^{-6}\max\{\hat{G}_k(\omega_f)\}$. Further evaluations revealed that, even better functionality may be achieved when this parameter has a random nature over the frequency line.

3.3.2 Detection of mode shapes

In addition to modal frequencies, the proposed method may also be used for detection of actual mode shape vectors. The quantities estimated using the approximate mode shape vectors of Fig. 4, are plotted in Fig. 3. The comparison between exact and estimated mode shapes shows a close accordance between these two quantities. Since the estimated mode shapes are more accurate compared to the initially assumed vectors, they may be used as new input to the proposed method to further improve the accuracy of the predictions.

3.3.3 Detection of damping ratios

The reference model with two different damping levels is used to evaluate the capability of proposed method in detection of modal damping. As reported by Rahman and Lau (2012) and also Schanke (2015), damping estimates from LSCF algorithm are not as reliable as frequency estimates and sometimes the errors can be significant. The same result was observed in the current study using Eq. (6) i.e., damping estimates were scattered. To get a better estimate of the damping ratios, the unknown parameters of the denominator polynomial are estimated directly from the Jacobian matrix [J] of Eq. (3) as a least squares problem. The detection is done using Eq. (16) and approximate mode shape vectors. Results for two first modes of both models are summarized in Table 1. Also, the stabilization diagram for the model with higher damping level is plotted in Fig. 6.

As it can be seen in the table, the proposed method is successful in detection of correct damping ratio corresponding to the selected mode shape vector. However, damping values are underestimated for all cases. Also, it should be mentioned that the coefficient of variation for the second mode is higher than the first mode for both models.

3.4 Detection of modal frequencies from noisy data

The next step in evaluation of eLSCF method is to see its performance in the presence of noise signals. The noise signals required for this purpose is produced synthetically by addition of 1000 sinusoidal curves with a mean frequency equal to μ_f and standard deviation equal to σ_f. Fig. 7 displays two examples of produced noises in time and frequency domains. The first plot contains a noise with a single average frequency and standard deviation (μ_f=10 Hz and σ_f=1 Hz), while the second signal include two peaks at two separate frequencies (μ_{f1}=5 Hz, μ_{f2}=10 Hz, $\sigma_{f1,2}$=1 Hz). Noise signals are added to the original records in time domain.

In the first attempt, a noise signal with a single peak (μ_f=10 Hz and σ_f=1 Hz) and signal to noise ratio (SNR) of 3.3, is added only to the first measurement channel (simulating electrical noise, malfunctioning sensor, operating mechanical devices, etc.). Fig. 8(a) displays auto-power spectrum of channel 1 after addition of the noise signal. The stabilization diagram constructed by LSCF method is presented in Fig. 8(b). According to the figure, the added noise appears as a pole in stabilization diagram making it difficult to distinguish between structural and nonstructural poles. However, as it can be seen in Fig. 8(c), the proposed eLSCF method is capable of detecting fundamental frequency for each vibration mode even in the presence of the noise signal and adoption of approximate mode shapes (α=1.0, using Eq. (16)).

The second case includes a separate noise signal in each measurement channel having two peaks at μ_{f1}=5 Hz and μ_{f2}=25 Hz ($\sigma_{f1,2}$=1 Hz) and SNR equal to 3.3. The auto-power spectrum of the measurement channels after addition of noise is presented in Fig. 9(a). The stabilization diagram corresponding to these noisy signals is calculated using LSCF method and presented in Fig. 9(b). Same as the

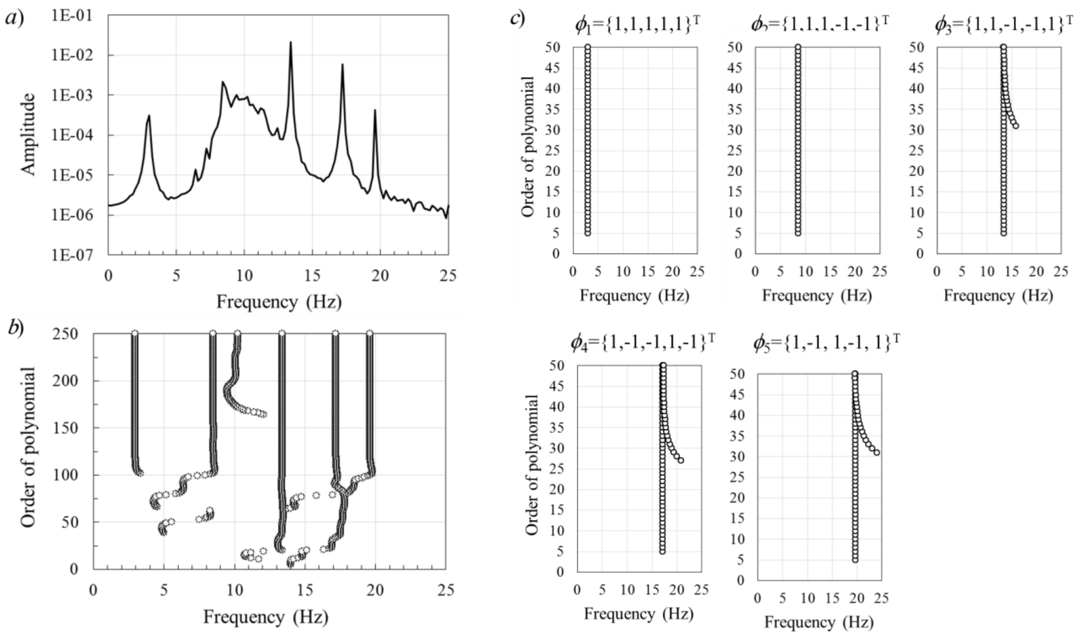

Fig. 8 Noise at channel 1 (μ_f=10 Hz and σ_f=1 Hz); (a) Auto-power spectrum of channel 1 after addition of noise; (b) Stabilization of natural frequencies from LSCF method; (c) Results of eLSCF method

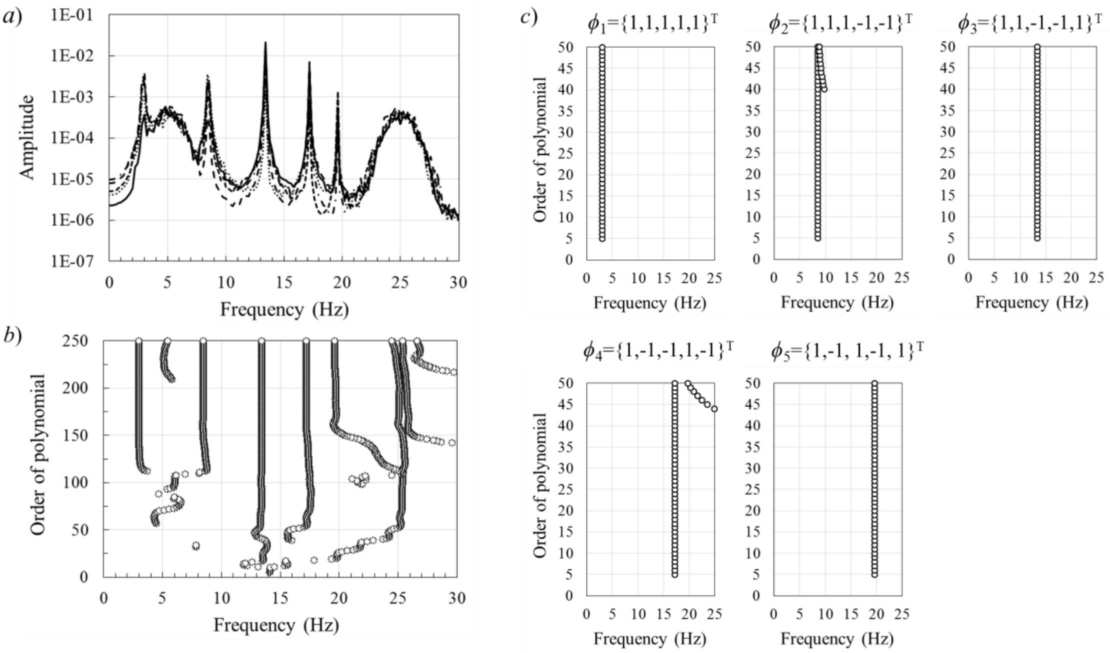

Fig. 9 Noise at all channels (μ_{f1}=5 Hz, μ_{f2}=25 Hz, $\sigma_{f1,2}$=1 Hz); (a) Auto-power spectra of measurement channels after addition of noise; (b) Stabilization of natural frequencies

previous case, additional poles appear at frequencies corresponding to the peaks of the noise signal. Fig. 9(c) shows results of eLSCF method using the approximate mode shapes (α=1.0, using Eq. (16)). According to the figure, the proposed method has a good capability in detection of modal frequencies by neglecting unwanted modes and noise signals.

3.5 Removing noise from original signal

As mentioned before, the proposed method may be utilized to remove noise signals from recorded data by adopting a negative value for the sensitivity exponent, α. In this case, the *CI* values calculated from Eq. (14) will vary from 1.0 (for most correlation) to infinity (for least correlation). Accordingly, Eq. (16) should be modified as it follows

$$CI_{new}(\omega_f) = \begin{cases} 0 & CI_{old}(\omega_f) < 1.25 \\ 1 & CI_{old}(\omega_f) \geq 1.25 \end{cases} \tag{18}$$

In above equation, different values may be used as *CI*

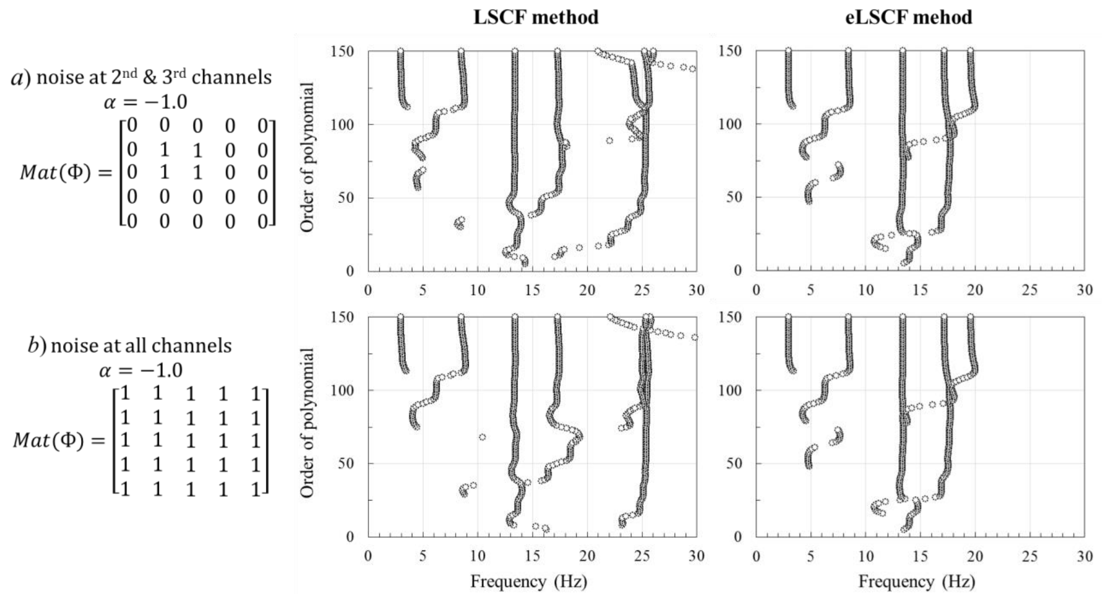

Fig. 10 Similar noises at (μ_f=25 Hz and σ_f=1 Hz); (a) 2nd & 3rd channels; (b) all channels

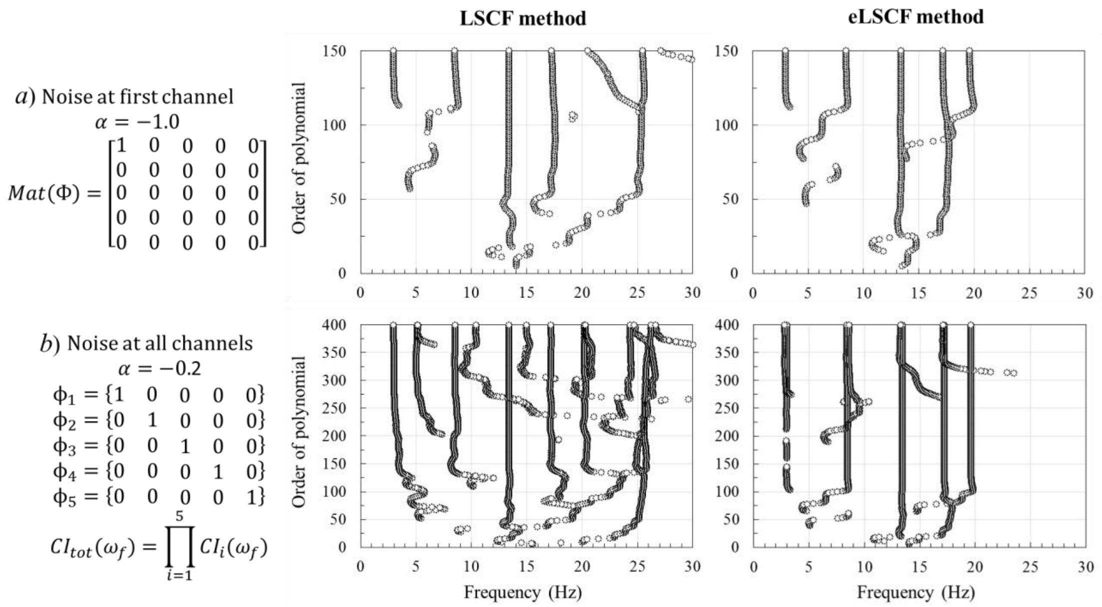

Fig. 11 Non-similar noise at recording channels; (a) noise at first sensor (μ_f=25 Hz and σ_f=1 Hz); (b) noise at all sensors (ch 1: μ_f=5 Hz; ch 2: μ_f=10 Hz; ch 3: μ_f=15 Hz; ch 4: μ_f=20 Hz; ch 5: μ_f=25 Hz; and σ_f=1 Hz)

rejection level. As the recorded signals may contain different types of noises, techniques for removing these contaminations are described in the following sub-sections.

3.5.1 Similar noises at recording channels

For recordings with similar noises at some channels, the pre-assumed modal vector should contain zeros at elements corresponding to non-noisy channels and ones at cells corresponding to noisy streams. Calculation of Φ vector should be done using Eq. (13) and *CI* should be obtained from Eq. (14) and Eq. (18). Fig. 10 displays two examples of data sets contaminated using a noise with μ_f=25 Hz, σ_f=1 Hz and SNR≈3.3. In the first set, only 2nd and 3rd channels are contaminated while in the second s*et al*l channels include the noise signal. For the data set containing noise at 2nd & 3rd channels, noise cleaning process is conducted using $\phi=\{0,1,1,0,0\}^T$. The resultant Φ vector is displayed in the matrix form in Fig. 10(*a*) from which it can be seen that, in addition to diagonal elements (auto-spectral), the cells corresponding to cross-spectral density of 2nd & 3rd channels are filled with ones meaning that the noise signals in 2nd & 3rd channels are correlated. For second data set (noise at all sensors), the appropriate noise removing vector will be in the form: $\phi=\{1,1,1,1,1\}^T$.

Comparing stability diagrams corresponding to LSCF and eLSCF methods, it can be seen that the proposed method is very efficient in detection of structural poles by rejecting the noise contamination. According to the left graphs (LSCF method), addition of noise to the recorded signals not only cause detection of an additional pole around 25 Hz, but also it diverts the pole corresponding to the 5th vibration mode. Meanwhile the plots corresponding to eLSCF method show stabilization of all structural poles without detection of any additional spurious pole.

3.5.2 Non-similar noises with different dominant frequencies

The noise contaminations of each sensor may originate from different sources resulting in non-similar noises with different dominant frequencies at recording channels. To study this case, let's consider the addition of a non-white noise only at one channel.

Fig. 11(a) displays the case in which the first channel contains a noise signal with μ_f=25 Hz, σ_f=1 Hz and SNR≈3.3. According to the previous sub-section, the appropriate vector for removing noise signal from this data set will be of the form $\phi=\{1,0,0,0,0\}^T$. As shown in the figure, the additional pole at 25 Hz that is reported by LSCF is removed using eLSCF and assumed noise removing vector. For data sets with other single noisy channels the similar noise removing vectors may be used (i.e., $\phi=\{0,1,0,0,0\}^T$ for 2nd channel, $\phi=\{0,0,1,0,0\}^T$ for 3rd channel, etc.). However, for the case in which multiple channels include non-similar noises with different dominant frequencies, the vector described in the previous sub-section will not work anymore. As an example, if the channels 3 and 4 contain non-similar noises, the vector $\phi=\{0,0,1,1,0\}^T$ will not be the correct selection, because the adoption of this vector means that the noise signals in 3rd and 4th channels have simultaneous auto-spectral peaks and are correlated to each other. Instead, this case can be treated as two single noisy channels with separate modal vectors, $\phi_1=\{0,0,1,0,0\}^T$ and, $\phi_2=\{0,0,0,1,0\}^T$.

To remove noise signals from both channels, the *CI* values calculated for individual noise removing vectors (from Eq. (18)) should be multiplied to each other as follows

$$CI_{tot}(\omega_f) = \prod_{i=1}^{j} CI_i(\omega_f) \tag{19}$$

where, $\prod$, is the product operator. Generally, for "*j*" number of recording channels containing non-similar noises with different dominant frequencies, the *CI* should be calculated "*j*" times using modal vectors corresponding to each individual channel. The total *CI* at each frequency will be computed from above equation.

Fig. 11(b) shows the application of this technique to remove the noise from a data set with non-similar noise at all recording channels (ch 1: μ_f=5 Hz; ch 2: μ_f=10 Hz; ch 3: μ_f=15 Hz; ch 4: μ_f=20 Hz; ch 5: μ_f=25 Hz; and σ_f=1 Hz). As it can be seen in the left graph, using traditional LSCF method five additional poles appear around the noise frequencies. However, the right graph shows that the proposed method is able to refine the polluted data set using the noise removing vectors presented in the figure. It is worth mentioning that when using negative, α, in Eq. (14), adoption of an exponent closer to zero makes the proposed method more efficient in removing noise signals. But care should be taken since if this value is selected very close to zero, it may cause deletion of some structural poles, too.

3.5.3 Uncorrelated noises with similar dominant frequency

Another case that can be encountered in OMA tests is the existence of uncorrelated noises with similar dominant frequency in different recording streams. As in this case, the noise signals existing in different channels are uncorrelated, it is not possible to use a single noise removing vector for all channels (as in sec. 3.5.1). Again, for each individual channel a separate modal vector should be considered, same as the previous sub-section. However, as in this case noisy channels will have simultaneous auto-spectral peaks, the *CI* for these noise removing vectors should not be calculated individually. Instead, the individual modal vectors calculated from Eq. (13) should be added up together prior to the calculation of *CI*

$$\Phi_{tot} = \sum_{i=1}^{j} \Phi_i \tag{20}$$

Once the total Φ vector is known, *CI* will be calculated

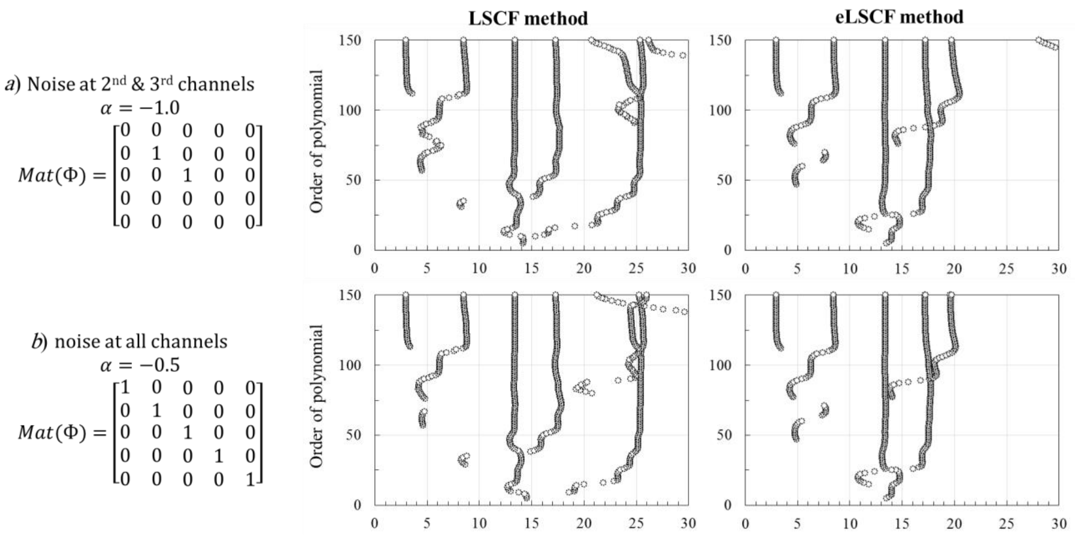

Fig. 12 Uncorrelated noises with μ_f=25 Hz and σ_f=1 Hz; (a) noise at 2nd & 3rd channels; (b) noise at all channels

using Eq. (14), and Eq. (18). Application of this procedure on two noisy data sets is illustrated in Fig. 12. The first set contains two different noises with μ_f=25 Hz, σ_f=1 Hz and SNR≈3.3 at 2nd & 3rd channels (Fig. 12(a)). The next set contains five different noises with same μ_f, σ_f and SNR at all recording channels (Fig. 12(b)). Each figure includes the resultant Φ vector in the matrix form according to which, it can be seen that only diagonal elements are filled with ones meaning that the noisy channels have simultaneous auto-spectral peaks. As the noise signals are uncorrelated, the cells corresponding to cross-spectral density (non-diagonal cells) are filled with zeros. Comparing results obtained from LSCF and eLSCF methods, it can be seen that the additional pole corresponding to the noise signal is omitted in the stability diagram of proposed method.

3.5.4 General case

In real applications, the recorded data may contain a mixture of above-mentioned noise types. As an example, a data set may include similar noises at all channels peaking at a certain frequency; meanwhile containing non-similar noises at some data lines peaking at other frequencies. Moreover, a data set may include two or more noises from one type (e.g., non-similar noises at 1st and 2nd channels peaking at f_1 plus non-similar noises at 2nd, 3rd and 4th channels peaking at f_2). For a data set including a mixture of noise types discussed in the former sub-sections, each noise type should be considered separately. Once the *CI* for each noise type is determined (from Eq. (18)), the total *CI* for all noises may be calculated using Eq. (19). By means of this *CI*, one can remove all considered noises from recorded data and obtain real structural poles.

4. Conclusions

The presence of measurement and other noises in structural output recordings requires refinement of recorded data to minimize their effects and eliminate them during detection of actual structural modes. This paper presents an enhanced version of LSCF method for determination of vibration properties from noisy data. The proposed method makes the use of pre-defined approximate mode shape vectors to refine the PSD matrix. For this purpose, a vector containing the correlation between predicted and measured C-PSD matrices (namely *CI*) was used to refine the measured data and eliminate effect of unwanted noises. A five story shear frame was adopted as the reference model to evaluate performance of eLSCF method in detection of modal properties using exact and approximate mode shapes. Based on the results, the enhanced method is capable of detecting modal frequencies even if the input mode shape vector is approximate. Also, it was shown that using eLSCF, the stabilization of diagrams starts even with a very low system order which shows the computational efficiency of the method. The natural frequencies found for the selected mode shape vectors were pretty accurate and close to the exact values. However, the damping ratios were harder to pick and estimates were not that good. The accuracy of eLSCF in detection of modal frequencies from noisy data was also examined. Evaluations showed that the proposed method is capable of detecting fundamental frequencies associated with the selected mode shape vector even in the presence of the noise signal. Also, the proposed method was utilized to remove noise signals from recorded data and noise removing techniques were discussed. Comparing results of LSCF and eLSCF methods, it was shown that the proposed method is very efficient in detection of structural poles by rejecting the noise contamination.

References

Aras, F. (2016), "Ambient and forced vibration testing with numerical identification for RC buildings", *Earthq. Struct.*, **11**(5), 809-822.

Au, S.K. (2017), *Operational Modal Analysis: Modeling, Bayesian Inference*, Uncertainty Laws, Singapore, Springer.

Bonness, W.K. and Jenkins, D.M. (2015), "Removing unwanted noise from operational modal analysis data", *Top. Modal Anal.*, **10**, 115-122.

Brincker, R., Ventura, C. and Andersen, P. (2003), "Why output-only modal testing is a desirable tool for a wide range of practical applications", *Proceedings of the International Modal Analysis Conference (IMAC) XXI*, Vol. 256.

Gouache, T., Morlier, J., Michon, G. and Coulange, B. (2013), "Operational modal analysis with non stationnary inputs", *IOMAC 2013*, Guimaraes, Portugal.

Jensen, H.A., Esse, C., Araya, V. and Papadimitriou, C. (2017), "Implementation of an adaptive meta-model for Bayesian finite element model updating in time domain", *Reliab. Eng. Syst. Saf.*, **160**, 174-190.

Masjedian, M. and Keshmiri, M. (2009), "A review on operational modal analysis researches: classification of methods and applications", *Proceedings of the 3rd IOMAC*, 707-718.

Mohanty, P. and Rixen, D.J. (2004), "Operational modal analysis in the presence of harmonic excitation", *J. Sound Vib.*, **270**(1), 93-109.

Ni, Y., Lu, X. and Lu, W. (2017), "Operational modal analysis of a high-rise multi-function building with dampers by a Bayesian approach", *Mech. Syst. Signal Pr.*, **86**, 286-307.

Ni, Y.Q., Zhang, F.L., Xia, Y.X. and Au, S.K. (2015), "Operational modal analysis of a long-span suspension bridge under different earthquake events", *Earthq. Struct.*, **8**(4), 859-887.

Ong, Z.C., Lim, H.C., Khoo, S.Y., Ismail, Z., Kong, K.K. and Rahman, A.G.A. (2017), "Assessment of the phase synchronization effect in modal testing during operation", *J. Zhejiang Univ., SCIENCE A*, **18**(2), 92-105.

Papadimitriou, C. and Papadioti, D.C. (2013), "Component mode synthesis techniques for finite element model updating", *Comput. Struct.*, **126**, 15-28.

Peeters, B. and De Roeck, G. (2001), "Stochastic system identification for operational modal analysis: a review", *J. Dyn. Syst. Measur. Control*, **123**(4), 659-667.

Peeters, B., Cornelis, B., Janssens, K. and Van der Auweraer, H. (2007), "Removing disturbing harmonics in operational modal analysis", *Proceedings of International Operational Modal Analysis Conference*, Copenhagen, Denmark.

Qin, S., Wang, Q. and Kang, J. (2015), "Output-only modal analysis based on improved empirical mode decomposition method", *Adv. Mater. Sci. Eng.*, **2015**, Article ID 945862, 12.

Rahman, M.S. and Lau, D. (2012), "Comparison of system identification techniques with field vibration data for structural health monitoring of bridges", M.Sc. Dissertation, Carleton University, Ottawa.

Rainieri, C. and Fabbrocino, G. (2014), *Operational Modal*

Analysis of Civil Engineering Structures, Springer, New York.
Reynders, E. (2012), "System identification methods for (operational) modal analysis: review and comparison", *Arch. Comput. Meth. Eng.*, **19**(1), 51-124.
Rodrigues, J., Brincker, R. and Andersen, P. (2004), "Improvement of frequency domain output-only modal identification from the application of the random decrement technique", *Proceedings of the 23rd Int. Modal Analysis Conference*, Deaborn, MI.
Schanke, S.A. (2015), "Operational modal analysis of large bridges", Master Thesis, NTNU-Norwegian University of Science and Technology.
Shouyuan, Z., Yimin, Z., He, L. and Bangchun, W. (2008), "Identification of noise modes for automobile operational modal analysis", *Int. J. Vehicle Noise Vib.*, **4**(4), 304-316.
Yu, D.J. and Ren, W.X. (2005), "EMD-based stochastic subspace identification of structures from operational vibration measurements", *Eng. Struct.*, **27**(12), 1741-1751.
Zhang, F.L. and Au, S.K. (2016), "Fundamental two-stage formulation for Bayesian system identification, Part II: Application to ambient vibration data", *Mech. Syst. Signal Pr.*, **66**, 43-61.
Zhang, F.L., Ni, Y.C. and Lam, H.F. (2017), "Bayesian structural model updating using ambient vibration data collected by multiple setups", *Struct. Control Hlth. Monit.*, **24**(12), e2023.
Zhang, F.L., Ni, Y.Q., Ni, Y.C. and Wang, Y.W. (2016), "Operational modal analysis of Canton Tower by a fast frequency domain Bayesian method", *Smart Struct. Syst.*, **17**(2), 209-230.
Zhang, F.L., Ventura, C.E., Xiong, H.B., Lu, W.S., Pan, Y.X. and Cao, J.X. (2018), "Evaluation of the dynamic characteristics of a super tall building using data from ambient vibration and shake table tests by a Bayesian approach", *Struct. Control Hlth. Monit.*, **25**(4), e2121.
Zhang, L., Brincker, R. and Andersen, P. (2005), "An overview of operational modal analysis: major development and issues", *1st International Operational Modal Analysis Conference (IOMAC)*, Copenhagen, Denmark.

CC